The Role of Common Cell Culture Media Supplements on the Nanoparticle Protein Corona Formation, Aggregation State, and the Consequent Impact on Cellular Uptake.

Francesco Barbero[a,b], Sara Michelini[c], Oscar H. Moriones[a,b], Javier Patarroyo[a], Jordi Rosell[d], Muriel F. Gustà[d], Michele Vitali[d], Luna Martín[e], Francesc Canals[e], Albert Duschl[c], Jutta Horejs-Höck[c], Laura Mondragón[a,d], Neus G. Bastús[a], Víctor Puntes *[a,b,d,f]

[a] Catalan Institute of Nanoscience and Nanotechnology (ICN2), CSIC and BIST, Campus UAB, Bellaterra, 08193 Barcelona, Spain

[b] Universitat Autònoma de Barcelona (UAB), Campus UAB, 08193, Bellaterra, Barcelona, Spain

[c] University of Salzburg, Department of Biosciences, Hellbrunner Str. 34, Salzburg, Austria

[d] Vall d'Hebron Institut de Recerca (VHIR), 08035, Barcelona, Spain

[e] Proteomics Laboratory, Vall d'Hebron Institute of Oncology (VHIO), Barcelona, Spain

[f] Institució Catalana de Recerca i Estudis Avançats (ICREA), P. Lluís Companys 23, 08010 Barcelona, Spain

Keywords

Protein Corona; gold nanoparticles, cell culture media, antibiotic, cellular uptake, NPs aggregation

Abstract

Sodium citrate-stabilized gold nanoparticles are destabilized when dispersed in cell culture media. This may promote their aggregation and subsequent sedimentation or, in the right conditions, their interaction with proteins leading to the formation of a stabilizing protein corona. Cell culture media are ionic solutions that contain nutrient growth substances and are typically supplemented, in addition to serum, with different substances such as dyes, antioxidants, and antibiotics. In this study, the impact of phenol red, penicillin-streptomycin, L-glutamine, and β-mercaptoethanol on the formation of the nanoparticle protein corona in cell culture media was investigated. Similar protein coronas were obtained except when antibiotics were present. The protein corona took more time to be formed in this condition, and its density and composition were altered, as UV-vis spectroscopy, Z potential, dynamic light scattering, and liquid chromatography-mass spectrometry analysis indicated. As a consequence of these results, a significantly different AuNPs cellular uptake was measured, showing that NP uptake

increased as did the NP aggregates. AuNP uptake studies performed in the presence of clathrin and caveolin mediated endocytosis inhibitors showed that neither clathrin receptors nor lipid rafts were significantly involved in the internalization mechanism. These results suggested that NPs aggregation was the principal responsible for NP cell uptake.

Introduction

The interaction of NPs with biological materials in physiological media and the ability of NPs to absorb and get coated with proteins forming a corona [1] has spurred significant efforts to understand its formation kinetics and nature [1]. This is because what ultimately living systems encounter is a hybrid object composed of an inorganic core and a protein coating. Consequently, it has been observed how the interaction with cells strongly depends on the composition and density of the proteins coating the NPs [2], their on-NP conformation [3], and the shaded and exposed area of the absorbed proteins [4].

From the NP point of view, when it enters physiological media, it is driven out of equilibrium, and then, it evolves towards a more stable state, reducing its high surface energy by the aggregation to other particles or conjugation with proteins present in the media. [5]. Note that the formation of a Protein Corona (PC) enveloping the NPs provides the actual biological identity. Consequently, it has crucial implications on biocompatibility, nanosafety, and NPs use in medicine [6–11].

The hardening is the PC formation, a time-dependent process. It starts from a "soft", transient, corona where only a weakly bound layer of proteins adsorbed on the particles surface, stabilizing the colloid in the saline medium but being in dynamic equilibrium with the unbound ones in solution evolving into a "hard" corona. Through different mechanisms, proteins form a strong stable bound permanent layer onto the surface of NPs [1,12], recalling somehow the "Vroman effect" [1,12]. In the sixties, Leo Vroman showed how adsorption of blood serum proteins to an inorganic surface is time-dependent, a hierarchical competitive adsorption process where the proteins with higher mobility are the first to reach the surface and are subsequently replaced by others with lower mobility but higher affinity [13–17]. In the case of NPs, the main differences with the previously studied surfaces are their high curvature and their Brownian dispersibility in the protein solution (Vroman surfaces where immobilized). Beyond the different crowding effects and re-arrangement of proteins at the NP surface also leads to a hardening of the protein corona without changing composition [7].

Due to the necessity to evaluate biological effects of NPs, especially their potential toxicity and their recognition by the immune system [18,19], many studies have been performed on the NPs PC formed in cell culture media (CCM) supplemented with serum, normally human serum or fetal bovine serum (FBS) are used. The formation of this NPs PC depends on both the NPs composition [20], size [21], shape [22], surface state [23], and the presence of different ions and molecules to varying concentrations in the incubation media [21]. Thus, most of the studies have been focused on the characteristics, and the type and concentration of proteins, while the role of other components present in the CCM have not been fully explored. CCM are complex media composed not only of salts and proteins but also of several supplements as vitamins, amino acids, sugars, pH indicator dyes, antioxidants and antibiotics. Moreover, different CCMs (e.g. RPMI, DMEM, MEM) present a different composition that significantly varies in the components and salts concentrations, factors that ultimately determine how the water envelop (following Debye length and the Hoffmeister series) surrounds NPs and proteins, which determine the NP-protein interactions [24,25].

In this context, gold nanoparticles (AuNPs), one of the most widely used materials in nanomedicine research for drug delivery, diagnostics, and therapy [26,27], has also been a model material to study the formation of the PC [1], thanks to its surface state and chemical environment-dependent plasmonic properties. In the present work, we explore the impact of several widely used CCM supplements on the formation process of the PC and the consequent NP-cell interaction.

Results and Discussion

Generally, when pristine (sodium citrate-coated) AuNPs and different CCM are mixed, two different kinetic processes are competing at the same time: the destabilization/aggregation of the NPs promoted by the high ionic strength of the media and the stabilization of the NPs surface against aggregation via proteins adsorption [1,21]. This is so that in the highly ionic physiological media, failing to make a PC, leads to irreversible aggregation and sedimentation of NPs, which has a dramatic impact on biological responses. The adsorption kinetics of proteins onto different AuNPs have been well described previously, indicating how different NPs, and different NP-CCM mixtures, follow different hardening processes [20].

Thus, synthesized AuNPs have been exposed to CCM complemented with different supplements. RPMI medium supplemented with 10% FBS was chosen as CCM. Supplements were added at the typical standard concentration used in the cell cultures. Four of them have been selected: Phenol Red (PhR), used as pH indicator, Penicillin/Streptomycin (PS), two antibiotics to prevent bacterial growth, L-glutamine (GLN), a polar amino acid used as a non-toxic source of nitrogen, and as a building block for the production of glutamate [28], and β-mercaptoethanol (BME), added to prevent toxic levels of ROS [29].

The evolution of AuNPs after exposure to the different media was characterized by resolving UV-vis spectroscopy, Z potential, and dynamic light scattering analysis (DLS). In the study of the evolution of NPs PC, the presence of free proteins in the solution can interfere. Therefore, purification after exposure to remove unbound protein is recommendable [1]. Additionally, the purification process gives an indication of the degree of protein coating (soft corona instead of the hard corona), since poorly coated NPs do not resuspend from the pellet after the centrifugation test.

In the present study, highly monodisperse citrate-stabilized gold nanoparticles of 24.0 ± 2.3 nm in diameter have been synthesized following reported kinetically controlled seeded-growth approach [30]. Due to its weak interaction with the gold surface [31], citrate is easily replaced by more affine species such as serum proteins [1]. In Figure 1, bright field scanning transmission electron microscopy (STEM) images, UV-vis absorption spectra, DLS, and Z potential of the used AuNPs are reported (black dash lines). The high monodispersity of the NPs allowed observing minor modifications of the PC formation process. Then, these AuNPs, at a concentration of $2.7 \cdot 10^{12}$ NPs/mL, were diluted 1:10 into CCM. The samples were purified by centrifugation before being measured and resuspended in sodium citrate 2.2 mM. In the UV-vis spectra of the AuNPs exposed to the CCM, a red-shift of the localized surface plasmon resonance (LSPR) peak and an increase of the absorbance were observed (Figure 1B), indicating the formation of a dense dielectric layer onto the NPs surface consistent with the dense absorption of proteins [1,32]. DLS evidenced an increase in the hydrodynamic size of about 20 nm, consistent with the formation of a protein monolayer. At short times, a higher diameter value by DLS was observed, attributable to the lesser colloidal stability of the NPs through the purification process at short times, which leaded to a small partial aggregation only observed by DLS since it is really sensible to aggregates (Figure 1C). Z potential showed a decrease in the surface charge of the NPs after their exposition to CCM, reaching already at the first measurements similar protein values of – 25 mV (at 0.30 mS/cm^2), an indication of a serum protein coating of the AuNPs surface.

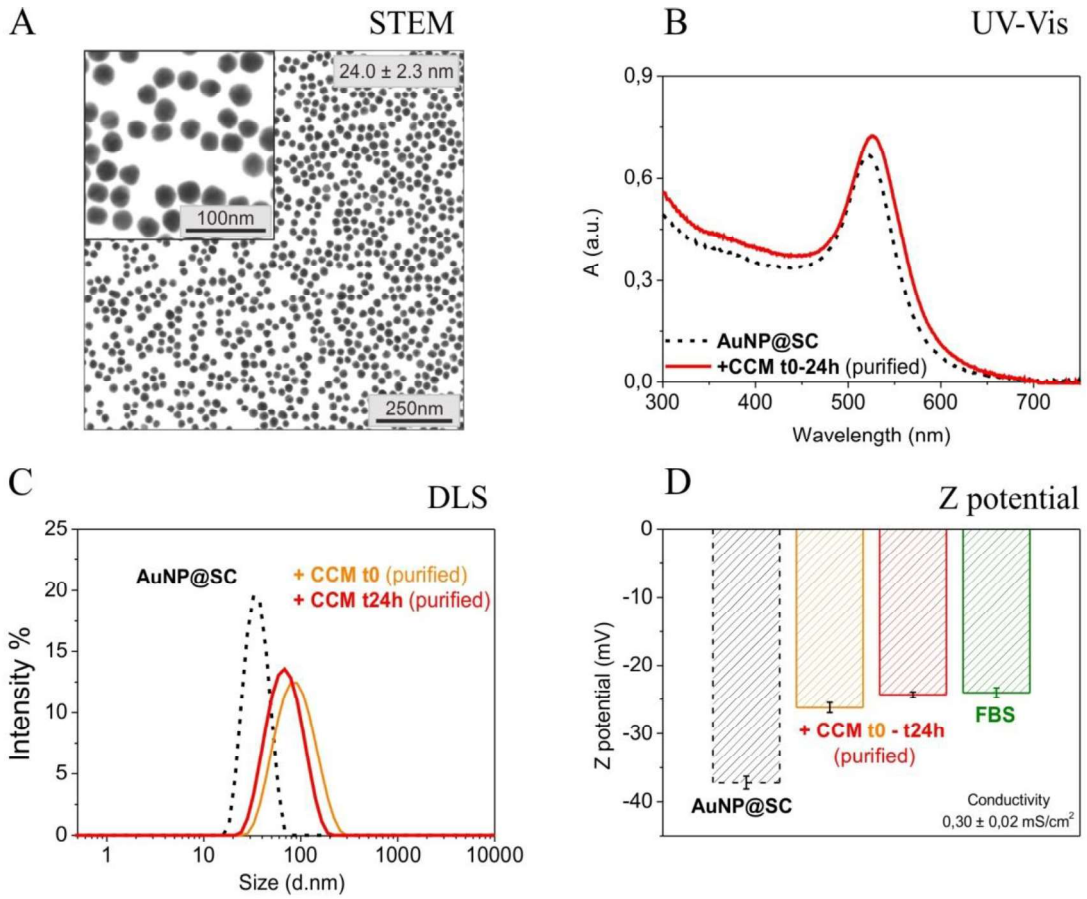

Figure 1. (**A**) Bright field STEM images of AuNPs. (**B-D**) Physicochemical characterization of AuNPs protein corona formation. (**B**) UV-vis spectra of AuNPs (black dash line), UV-vis spectra of AuNPs at time 0 and after 24h of exposition to CCM purified by centrifugation (red solid line); (**C**) DLS (by intensity) of: AuNPs (black dash line) and AuNPs at time 0 and after 24h of exposition to CCM purified by centrifugation (orange and red solid line, respectively); (**D**) Z potential of: AuNPs (black dash line); AuNPs at time 0 and after 24h of exposition to CCM purified by centrifugation (orange and red solid line, respectively) and partially dialyzed (against 2.2mM Na citrate) FBS (green solid line) all the samples presented similar pH and conductivity (0.30 ± 0.02 mS/cm^2).

Next, we observed the spectroscopic features of the PC formed in the presence of the different cells culture supplements at standard concentrations. In Figures 2A and 2B the UV-vis and DLS profiles of the formed PC in CCM and CCMs complemented with GLN, BME or PhR (2 mM; 50 μM and 44.8 μM, respectively) are reported. Interestingly the presence of the above-mentioned CCM supplements did not influence the formation of the PC. On the contrary, all of them showed spectral features and hydrodynamic diameters very similar to that of the additive-free media, denoting high robustness and reproducibility of the applied procedure. However, a clear different behavior was observed in the presence of PS (Figure 2B, C). When the PS was present at 1% (~ 170 μM penicillin, 172 μM streptomycin), the UV-vis profile showed, immediately after the addition of the NPs to the CCM, the appearance of a shoulder at ~ 650 nm typical of NP's aggregation, attributed to inter-particle plasmon

coupling [33]. Interestingly, the degree of the aggregation did not substantially increase over time (data not shown), indicating that after aggregation, the system reached a stable state. When samples were purified, the resultant UV-vis spectra (Figure 2C, blue dash) clearly showed increased aggregation, indicating less protected NPs. The DLS of the unpurified sample presented an increase in the hydrodynamic diameter ascribable to the presence of NP aggregates (Figure 2B). Regardless of the aggregation state, the surface charge of these aggregates is similar to that of non-aggregated samples, suggesting that during or after NP aggregation, proteins finally coat the NPs and their aggregates, showing that in the presence of PS the aggregation of NPs is faster than the protein conjugation. The NPs destabilization in the occurrence of PS may be due to the cationic nature of the streptomycin, which was observed to induce strong aggregation once AuNPs were exposed to a simple PS aqueous solution (Figure 1-SI D). Conversely, the other tested supplements were also able to interact with the AuNPs but without compromising the NPs colloidal stability, just a partial destabilization in the case of BME was perceived (Figure SI-1A, B, C).

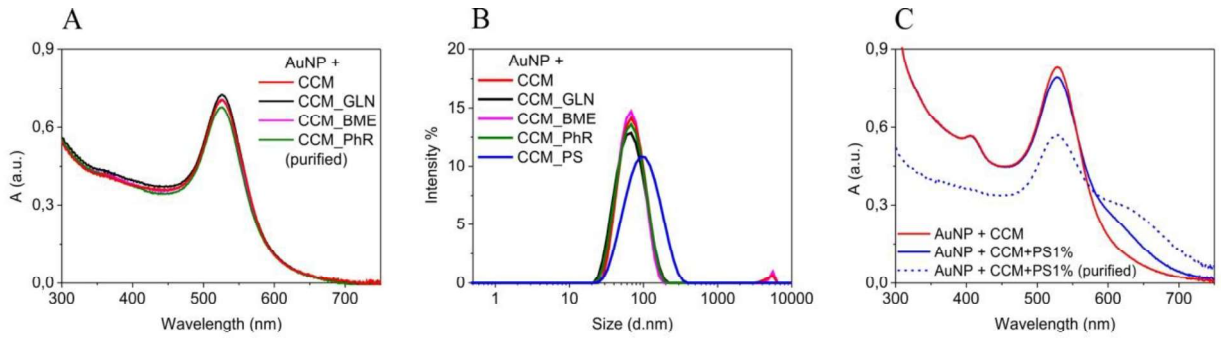

Figure 2. Effects of the addition of CCM supplements to CCM on NP PC formation. (**A**): UV-vis spectra of AuNPs exposed to CCM (red); UV-vis spectra of AuNPs exposed to CCM + GLN/BME/PhR (black, purple, green, respectively) the samples were purified before being measured. (**B**): DLS (by intensity) of AuNPs: 24h of exposition with CCM (red), CCM + GLN/BME/PhR (black, purple, and green, respectively) and CCM + PS (blue). (**C**): UV-vis spectra of AuNPs exposed to CCM (red), AuNPs exposed to CCM + 1% PS before purification (blue) and after purification (blue dash).

Thus, when NPs were exposed to CCM complemented with a growing concentration of PS (1%, 5% and 10%), a second plasmonic peak was observed. The extent of the aggregation was quantified from UV-vis spectra by calculating the Aggregation Parameter (AP) according to Lévy et al. [34]. AP values higher than 0.5 indicated significant aggregation. The results showed that the aggregation increased as the PS concentration increase (Figure 3A, blue bars). The extent of these aggregations was variable (outcome of 5 repetitions) but consistent with the observed trend. As expected, no influence of the PS presence on the AuNPs surface charge was detected (Figure 3A, black squares). The Z potential value corresponded to that of a protein layer on the AuNPs; however, it was not possible to exclude the

presence of PS in the corona since it may be buried (masked) crosslinking the negative NP surface and protein surface charges.

The time evolution of the "hard" PC formation was followed by UV-vis spectroscopy measuring the extent of the LSPR red-shift of the AuNPs once exposed to CCM and CCM complemented with 1% PS after purification (Figure 3B). In this study, the concentration of AuNPs was decreased to the 50% of the initial value ($1.4 \cdot 10^{11}$ NPs/mL in CCM) to reduce the NPs aggregation rate previously observed and hence to interpret the UV-vis results better. In these conditions but in the absence of PS, a "hard" PC (resistant to purification cycles) was observed from the initial time. Conversely, much slower time evolution of the LSPR peak was noted if PS was present in the CCM. Thus, a partial red-shift was detected at time 0, and the system needed at least 20 h to reach a stable condition (Figure 3B, blue circles). The observed difference in the time evolution of the PC hardening process in presence of PS could be ascribed to a slower rearrangement of the proteins during the corona formation. The time evolution of the Z potential value of the purified samples did not show any significant differences once PS was present (Figure 3C). Still, as already discussed, an eventual presence of the PS in the AuNPs PC should not influence the overall surface charge.

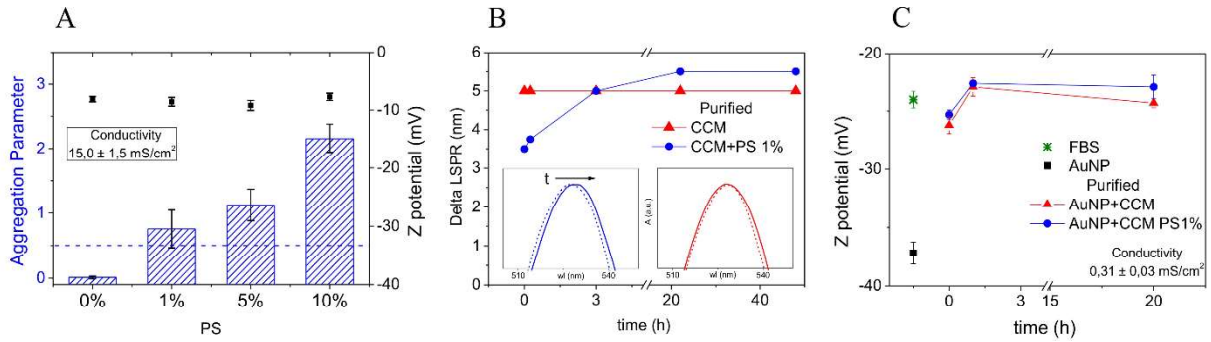

Figure 3 Effects of the addition of PS to CCM on the time evolution of nanoparticle PC formation. (**A**) Experimentally measured Aggregation Parameters (AP) of AuNPs exposed to CCM with growing concentration of PS (blue bars), AP values higher than 0.5 indicated significant aggregation. Z potential of the same sample not purified (conductivity 15.0 ± 1.5 mS/cm^2) (black square). (**B**) Time evolution of the Protein Corona formation followed by the LSPR red shift: Delta LSPR of AuNPs exposed to CCM (red triangle) and exposed to CCM added of 1% PS (blue circle). All the samples were purified by centrifugation. UV-vis spectra of the time 0 and time 22 h of the 2 samples. (**C**) Z potential of: FBS (green); AuNPs (black); AuNPs exposed to CCM (red); AuNPs exposed to CCM + PS (Blue). All the samples were purified and present similar pH and conductivity (0.31 ± 0.03 mS/cm^2).

To further investigate the consequences of the presence of PS during the formation of the NPs PC, liquid chromatography mass spectrometry (LC-MS) analysis of the proteins composing the PC in presence and absence of 1% PS was performed. AuNPs were exposed to CCM and to CCM

complemented with 1% PS, aged 48h prior to being purified by centrifugation (5 cycles) to remove all not bound proteins, and finally processed for the LC-MS analysis. More than 140 serum corona proteins were identified, and a semi-quantitative analysis was performed. Looking at the relative abundances of the whole identified proteins, grouping them for mass, it was also possible to conclude that the two PC (in the presence and absence of PS) presented a different composition (Figure 4C). In the sample incubated in CCM plus PS, the most abundant protein was the S100A12 (a metal ion binding protein). On the contrary, in the sample incubated with CCM, the bovine albumin is the most abundant one. Besides, 14 proteins out of the top 20 were in commonly found in all analyzed samples but with different order and relative abundance (Figure 4A, B; Table 1). Also, grouping the proteins for their isoelectric point (IP) suggested how the PS influences the PC formation. In addition, the LC-MS analysis showed that proteins possessing a negative charge at the CCM (pH 7.4) represented far more the majority of the proteins present in both coronas. This result was in good agreement with the measured Z potential value. The presence of the cationic PS may lead to higher negative values due to the PS cationic charge calling for more negatively charged proteins at physiological pH. Performed LC-MS results were ulterior evidence of the antibiotic interfering ability in the corona formation, highlighting that it also affected the final protein composition.

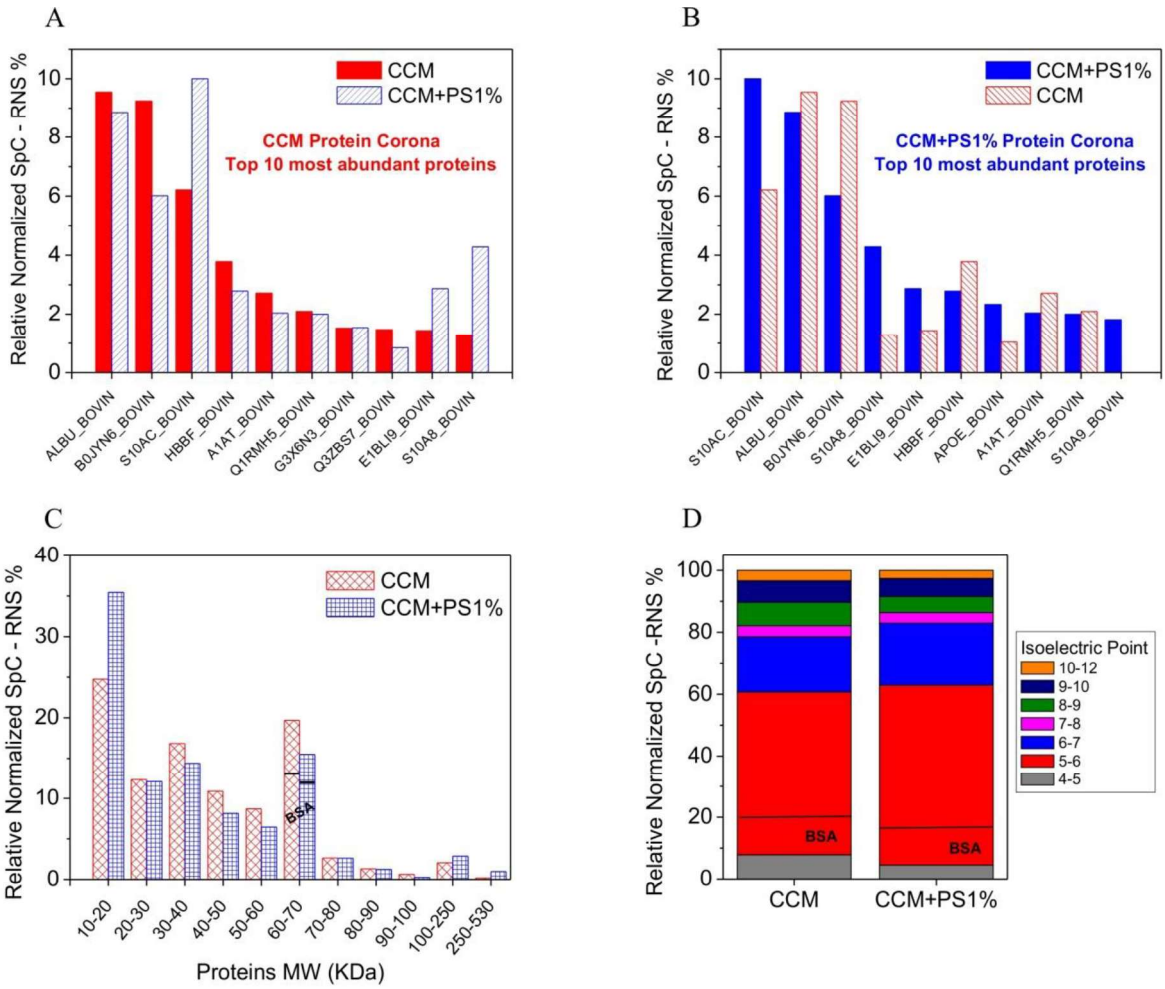

Figure 4. Classification of corona proteins identified on AuNPs exposed to CCM and CCM supplemented with 1% PS by LC-MS analysis. (A) Relative Normalized Spectral Counts (RNS) of the Top 10 most abundant proteins composing the PC resultant of AuNPs exposure to CCM (full red) compared with the Relative Normalized Spectral Counts (RNS) of the same proteins in the PC resultant of the exposure to CCM+PS1% (blue lines). (B) *Vice versa* the RNS of the Top 10 most abundant proteins composing the PC resultant of AuNPs exposure to CCM+PS1% (full blue) compared with the RNS of the same proteins in the PC resultant of the exposure to CCM (red lines). (C) Proteins composition RNS percentage of the two PC grouped for molecular weight. (D) Proteins composition percentage of the two PC grouped for isoelectric point.

CCM	MW (KDa)	IP
ALBU_BOVIN	69.2	5.8
B0JYN6_BOVIN	38.4	5.2
S10AC_BOVIN	10.7	5.9
HBBF_BOVIN	15.8	6.6
A1AT_BOVIN	46.1	6.1
Q1RMH5_BOVIN	29	8.8
G3X6N3_BOVIN	77.6	7.1
Q3ZBS7_BOVIN	53.5	5.9
E1BLI9_BOVIN	16.4	6.3
S10A8_BOVIN	10.5	5
K1C10_BOVIN	54.8	4.9
C1QB_BOVIN	26.4	10.2
C1QA_BOVIN	25.8	9.9
G5E513_BOVIN	49.9	5.3
F1MSZ6_BOVIN	52.4	6.4
APOE_BOVIN	36	5.4
E1B6Z6_BOVIN	23	9.4
KNG2_BOVIN	68.7	6.1
IPSP_BOVIN	45.3	9.9
MYL6_BOVIN	16.9	4.4

CCM+PS	MW (KDa)	IP
S10AC_BOVIN	10.7	5.9
ALBU_BOVIN	69.2	5.8
B0JYN6_BOVIN	38.4	5.2
S10A8_BOVIN	10.5	5
E1BLI9_BOVIN	16.4	6.3
HBBF_BOVIN	15.8	6.6
APOE_BOVIN	36	5.4
A1AT_BOVIN	46.1	6.1
Q1RMH5_BOVIN	29	8.8
S10A9_BOVIN	17.1	6.3
G3X6N3_BOVIN	77.6	7.1
APOA1_BOVIN	30.3	5.6
C1QA_BOVIN	25.8	9.9
F1MS32_BOVIN	21.4	5
HBA_BOVIN	15.2	9.1
C1QB_BOVIN	26.4	10.2
Q3ZBS7_BOVIN	53.5	5.9
G5E513_BOVIN	49.9	5.3
C4T8B4_BOVIN	25.3	6.4
E1BNR0_BOVIN	515.4	6.3

Table 1. Top 20 most abundant proteins in the two coronae, underlined in grey the proteins present in both columns.

It has been previously reported that the PC composition affects NP-cell interactions, particularly NPs internalization [35], and also how the NP aggregation state influences the cellular uptake [36,37]. The uptake efficacy was tested using ovarian cancer HeLa cells as a standard cell model widely used for similar studies [35,36,38]. AuNPs exposed for 24 h to CCM and CCM complemented with 1% PS were added at a final concentration of 2.7, 1.4, and 0.68 $\cdot 10^{11}$ NPs/mL. The experiment was performed 3 times each one in triplicates. Au quantification was determined by inductively coupled plasma mass spectrometry (ICP-MS). Despite this methodology is widely accepted, and ICP-MS can provide a good indication of the NP uptake, it does not discriminate between NPs internalized in the cells or attached to their surface. In order to minimize this interference, exhaustive cell washings were performed after NPs addition and incubation to remove those NPs located at the surface of the cells prior analysis [36,39,40].

The percentage in mass of the cellular uptake of AuNPs forming the PC in the presence or absence of 1% PS were similar at the lower concentration tested. Conversely at the highest concentration tested, an increase of uptake was detected (Figure 5A). As observed, the presence of PS, especially at a high concentration of NPs, led to the formation of NPs aggregates, and the extent of this aggregation was variable between different experiments (Figure 3A). Thus, the monitored increase in the uptake could

be attributed to the lower "solubility" of the sample due to the formation of AuNPs aggregates, and the variability of the aggregation state could explain the high standard deviation observed. As aggregation strongly depends on concentration, and PC formation on ratio between the NP's surface exposed and the total number of proteins [21], in the case of PS present in the media, this ratio has to decrease (number of proteins has to increase) in order to be able to stabilize the added NPs.

To assess this point, AuNPs aggregates of several diameters were prepared before exposure to HeLa cells (final NPs concentration of $2.7 \cdot 10^{11}$ NPs/mL). Five AuNPs samples were exposed to CCM without serum proteins for 1, 3, 5, 7, and 10 seconds before the addition of FBS. As described, in the absence of FBS the salty cell media led to NPs destabilization and aggregation. The aggregation process can be stopped by protein addition (Figure SI-2). Consequently, the addition of FBS to the samples at different times led to the formation of protein-stabilized AuNPs aggregates with different sizes and equal final AuNPs concentration (Figure 5B, red triangles, measured by DLS). Figure 5B shows the percentage of uptake in mass of each AuNPs aggregate sample. As the AuNPs aggregate mean size increased, the percentage of Au taken also increased. This finding could be explained with a major interaction NP-cell due to a slower Brownian motion of larger aggregates and faster flocculation. The results suggested that the increase in the uptake of AuNPs diluted into CCM+PS could be due to the presence of NPs aggregates rather than a different PC composition.

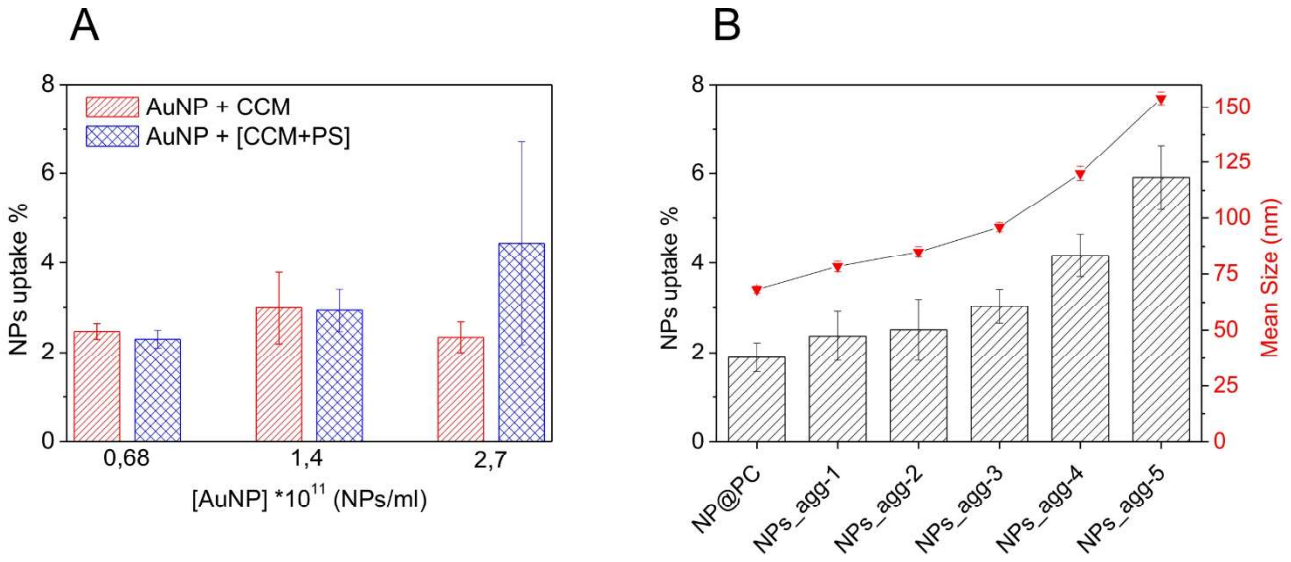

Figure 5. NPs cell uptake studies. ICP-MS analysis of the Au content present in HeLa cells after the exposure to AuNPs and after 3 washing steps with PBS; the content it is expressed in percentage of mass respect to the initial AuNPs *concentration*. (A) AuNPs + CCM (red lines); AuNPs + [CCM+PS] (blue rhombus) % uptake after the cell exposure to 2.7, 1.4, $0.68 \cdot 10^{11}$ NPs/mL. (B) Uptake % of AuNPs aggregates (black bars); mean size (by intensity) determined by DLS of AuNPs aggregates (red triangles).

Finally, we investigated if the uptake mechanism involved a specific recognition of the proteins which composed the PC in the presence or absence of PS. For that purpose, chlorpromazine, an inhibitor of clathrin-mediated endocytosis, and genistein, an inhibitor of caveolae-mediated endocytosis, were chosen. They have been previously used to investigate receptor mediated NP endocytosis [35]. Despite not being specific inhibitors of both pathways, their use can give us some hints about the mechanisms that may be involved in NPs internalization and the possible effect of different PC in this process. Prior their use, cytotoxicity tests of the inhibitor were performed to determine its maximum non-toxic concentration which were similar to the ones previously reported in the literature [35] (data not shown). Thus, AuNPs were first exposed for 24h to CCM with and without PS, then the samples were exposed to the cells previously incubated 1 h with the corresponding inhibitor. After 2 h of exposure, NPs were removed, and the cells were exhaustively washed with PBS (3 cycles) in order to remove non-internalized NPs, and cell pellets were collected for the ICP-MS analysis. Results showed that the extent of uptake was not subjected to significant changes when the inhibitors were added compared to the control samples, both for AuNPs exposed to CCM and CCM+PS (Figure 6), indication of a non-specific uptake mechanism involved.

Indeed, in the case of cells treated with NPs exposed to CCM+PS and caveolin inhibitor, genistein, a discrete increase in cellular uptake was observed. That could be explained by “cross-regulation” mechanism in which inhibition of an endocytic pathway may induce up-regulation of alternate pathways [41,42]. Thus, leading to a rather complex scenario where blocking of an uptake route is compensated by alternative pathways [43]. In any case, this study confirms that the differences observed in the PC composition were not responsible for the various degrees of uptake, rather, this phenomenon depended mainly on flocculation and diffusion velocities of the NPs.

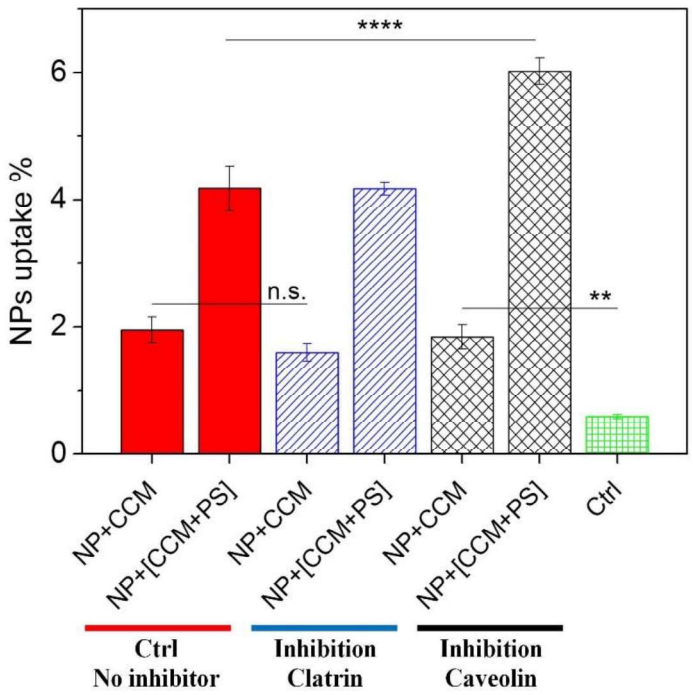

Figure 6. Effect of clathrin and caveolin mediated endocytosis inhibition on the uptake (on HeLa cells) of AuNPs exposed to CCM and CCM+PS. Statistical analysis was performed using ANOVA test combined with Tukey's test ($p < 0.01$ **, $p < 0.0001$ ****).

Conclusions

The results of this study showed that different common additives employed in CCM could affect the formation process of the AuNPs PC and its final composition. In particular, the widely used PS proved to have a significant impact in this regard. The presence of the antibiotic, especially at high NPs concentrations, led to NPs aggregation, which influenced the NP-cell interactions. NPs uptake studies in presence of two endocytic pathway inhibitors (clathrin and caveolin pathways) indicated that the different composition of the PC did not affect the cellular uptake. On the contrary, cellular uptake studies signaled that, the increase of size of the NP aggregates was the leading force for a major uptake. This phenomenon was associated with the faster sedimentation rate and the slower Brownian motion of larger aggregates that increased their interaction with cells. These studies indicated the importance of considering the NP aggregation state for *in vitro* and *in vivo* tests. This work also further highlighted the importance of characterizing the NPs evolution in biological media to correctly interpret NP-cell studies, correlating the features of the final nano-object with the cell response.

Materials and Methods

Chemicals.

Tetrachloroauric(III) acid trihydrate (99.9% purity), sodium citrate tribasic dihydrate (≥99%), RPMI-1640 R7509 (with sodium bicarbonate, without L-glutamine and phenol red, liquid, sterile-filtered, suitable for cell culture), Phenol Red (powder, suitable for cell culture), Penicillin-Streptomycin (Solution stabilized, with 10,000 units penicillin and 10 mg streptomycin/mL, sterile-filtered, BioReagent, suitable for cell culture), L-glutamine and β-mercaptoethanol (≥99.0%) were purchased from Sigma-Aldrich. Fetal Bovine Serum, FBS (research grade, triple 0.1 micron filtration) was purchased from ThermoFisher scientific. All reagents were used as received without further purification, all plastic material was sterile grade and all glass material was sterilized in an oven prior to use. Autoclave sterilized Milli-Q water was used in the preparation of all solutions. Cell culture medium (CCM) consisted of RPMI supplemented with 10% of FBS. Au NPs and CMM complemented with different reagents were mixed and placed in an incubator at 37°C for different incubation times.

Nanoparticle Synthesis and Purification.

Aqueous solution of citrate-stabilized AuNPs were synthesized according to the previously developed seeded-growth method in our group [30]. Briefly, 150 mL of sodium citrate aqueous solution was brought to a boil in a three necks flask under reflux, subsequently 1 mL of 25 mM $HAuCl_4$ was injected in the citrate solution. After a few minutes, the solution becomes reddish, a synonymous of AuNP formation (~ 10nm, seeds). Following sequential steps of growth, consisting of sample dilution plus further addition of gold precursor, the desired AuNP size was reached. **AuNPs purification** was performed centrifuging the NPs at 15000g for 15 min, removing 95% of the supernatant, followed by resuspension in the particle original medium (sodium citrate 2.2 mM).

Physicochemical Characterization of the NPs and NPs-Protein Corona.

AuNPs and the time evolution of their protein coating were characterized before and after exposure to CCM using different techniques. The proper combination of these techniques has been used in other similar studies by our group [1] and proven to be reliable when performed with adequate controls. **Electron Microscopy**. Diameter of the synthesized particles was obtained from analysis of Scanning Electron Microscopy (SEM) with FEI Magellan XHR SEM, in transmission mode operated at 20 kV. Samples were prepared by drop-casting 4μL of the sample on a carbon-coated copper TEM grid and left to dry at room temperature. At least 500 particles from different regions of the grid were counted. In order to avoid aggregation of the particles during TEM grid preparation they were previously

conjugated with 55KDa polyvinylpyrrolidone (PVP) [44]. **UV-vis Spectroscopy**. UV-vis spectra were acquired with a Shimadzu UV-2400 spectrophotometer. 1 mL of sample was placed in a plastic cuvette, and spectral analysis was performed in the 300−750 nm range at room temperature. UV-vis absorption spectra of AuNPs are due to NPs localized surface plasmon resonance (LSPR) that is the collective oscillation of the metallic surface electrons, highly sensitive to the NP environment. Local refractive index changes produce a shift of the LSPR, red-shifts are observed in case of a RI increase around metal, such as those induced by protein adsorption on NP, *vice versa* a RI decrease produce a blue-shift, therefore the changes in the close environment of the NPs can be investigated using this technique [45]. Water was taken as blank or reference for all samples. **Size and Zeta Potential Measurements**. The hydrodynamic diameter and Z potential of the AuNPs before and after incubation in CCM were determined by Dynamic Light Scattering, and Laser Doppler Velocimetry, respectively, using a Malvern Zetasizer Nano ZS instrument equipped with a light source wavelength of 632.8 nm and a fixed scattering angle of 173°. Diameters were reported as distribution by intensity calculated by non-negative least squares (NNLS) analysis. The software was arranged with the parameters of refractive index and absorption coefficient of gold, and solvent viscosity of water at 25°C.

Liquid chromatography-Mass spectrometry analysis (LC-MS)

Sample preparation and in-gel-digestion. The proteins composing the NP PC were then recovered by boiling for 10 min with 20 µL of 10% SDS, followed by centrifugation at 15000G for 20 minutes. The supernatant was separated and run on a 10% SDS-PAGE gel. Electrophoresis was stopped when the sample had run completely through the upper stacking gel, and about half a centimeter into the resolving gel. The gels were stained with colloidal Coomassie blue. The acrylamide sections containing the protein mixtures were cut from the gel and subjected to trypsin digestion using modified porcine trypsin (Promega, Madison, WI). Briefly, stained gel fragments were cut into small pieces, washed with 200 µL of 50 mM ammonium bicarbonate/50% ethanol for 20 min and dehydrated with 200 µL of 100% ethanol for 20 min. Reduction and alkylation was performed by incubating samples with 200 µL of 10 mM DTT in 50 mM ammonium bicarbonate for 1 h at 56°C, followed by alkylation with 200 µL of 55 mM Iodoacetamide in 50 mM ammonium bicarbonate for 30 minutes, protected from light. The gel pieces where then washed with 200 µL of 25 mM ammonium bicarbonate for 20 min, and dehydrated with 100 µL of acetonitrile for 10 min. Then 300 µL of 2.7 ng/µL trypsin in 25 mM ammonium bicarbonate solution was added to rehydrate and fully cover the acrylamide pieces. Trypsin digestion was run overnight at 37°C. Peptide extraction was carried out by addition of 150 µL of acetonitrile, followed by incubation for 15 min at 37ºC, and then addition of 500µL of 0.2% TFA, and further incubation for 30 min at r.t. The eluted peptides were dried in a SpeedVac and stored at -

20°C until analysis by liquid chromatography-mass spectrometry. **LC-MSMS analysis.** Tryptic digests (1/3 of the sample) were analyzed using a linear ion trap Velos-Orbitrap mass spectrometer (Thermo Fisher Scientific, Bremen, Germany). Instrument control was performed using Xcalibur software package, version 2.2.0 (Thermo Fisher Scientific, Bremen, Germany). Peptide mixtures were fractionated by on-line nanoflow liquid chromatography using an EASY-nLC 1000 system (Proxeon Biosystems, Thermo Fisher Scientific) with a two-linear-column system. Digestion mixtures were loaded onto a trapping guard column (Acclaim PepMap 100 nanoviper, 2 cm long, ID 75 μm packed with C18, 3 μm particle size from Thermo Fisher Scientific) at 4 μL/min. Then, samples were eluted from the analytical column (25 cm long, ID 75 μm packed with Reprosil Pur C18-AQ, 3 μm particle size, Dr. Maisch). Elution was achieved by using a mobile phase from 0.1% fluorhydric acid (FA) (Buffer A) and 100% acetonitrile with 0.1% FA (Buffer B) and applying a linear gradient from 5 to 35% of buffer B for 60 min at a flow rate of 300 nL/min. Ions were generated applying a voltage of 1.9 kV to a stainless steel nano-bore emitter (Proxeon, Thermo Fisher Scientific), connected to the end of the analytical column, on a Proxeon nano-spray flex ion source. The LTQ Orbitrap Velos mass spectrometer was operated in data-dependent mode. A scan cycle was initiated with a full-scan MS spectrum (from m/z 300 to 1600) acquired in the Orbitrap with a resolution of 30,000. The 20 most abundant ions were selected for collision-induced dissociation fragmentation in the linear ion trap when their intensity exceeded a minimum threshold of 1000 counts, excluding single charged ions. Accumulation of ions for both MS and MS/MS scans were performed in the linear ion trap, and the AGC target values were set to 1 × 106 ions for survey MS and 5000 ions for MS/MS experiments. The maximum ion accumulation time was 500 and 200 ms in the MS and MS/MS modes, respectively. The normalized collision energy was set to 35%, and one microscan was acquired per spectrum. Ions subjected to MS/MS with a relative mass window of 10 ppm were excluded from further sequencing for 20 s. For all precursor masses a window of 20 ppm and isolation width of 2 Da was defined. Orbitrap measurements were performed enabling the lock mass option (m/z 445.120024) for survey scans to improve mass accuracy. **Protein Identification.** LC-MS/MS data were analyzed using the Proteome Discoverer software (Thermo Fisher Scientific) to generate mgf files. Processed runs were loaded to ProteinScape software (Bruker Daltonics, Bremen, Germany) and peptides were identified using Mascot (Matrix Science, London UK) to search the SwissProt database, restricting taxonomy to bovin proteins. MS/MS spectra were searched with a precursor mass tolerance of 10 ppm, fragment tolerance of 0.8 Da, trypsin specificity with a maximum of 2 missed cleavages, cysteine carbamidomethylation set as fixed modification and methionine oxidation as variable modification. Significance threshold for the identifications was set to $p<0.05$ for the probability-based Mascot score,

minimum ions score of 20, and the identification results were filtered to 1% FDR at peptide level, based on searches against a Decoy database. Semi-quantitative comparison was made on the basis of the spectral counts (SpC) assigned to each protein. Spectral counts were normalized for total SpC on each LCMS run, to account for differences in sample load or MS signal. To compare the relative protein abundances in each sample, SpC numbers were divided by the molecular weight (MW) of the corresponding protein, to compensate for the number of theoretical tryptic peptides derived for each protein.

NP cellular uptake.

The experiments were performed per triplicate on 6 and 12 wells plates with approximately $1.25 \cdot 10^5$ and $6.25 \cdot 10^4$ cells/well respectively. CCM with no complements was added to 3 wells as controls on each experiment. The rest of the cells plated were incubated with CCM with or without PS at 1% in the presence of 2.7, 1.4 or $0.68 \cdot 10^{11}$ NPs/mL. The effect of NPs aggregation on cellular uptake was also tested by incubating HeLa cells in the presence of CCM with the 5 AuNPs aggregates samples - prepared as described above - all the samples contained $2.7 \cdot 10^{11}$ NPs/mL. Finally, the effect of clathrin mediated endocytosis was determined by employing chlorpromazine, which inhibits this endocytic pathway by preventing the assembly and disassembly of clathrin lattices on cell surfaces and on endosomes. The role of caveolae-mediated endocytosis was determined by using genistein, an inhibitor of tyrosine kinases involved in caveolae-mediated endocytosis. . Cells were pre-treated when indicated with chlorpromazine 10 μg/mL or genistein 200 μM for 1 h, prior removal of the media and the addition of $2.7 \cdot 10^{11}$ NPs/mL resuspended in CCM with or without PS and in the presence or not of chlorpromazine 10 μg/mL. After 2 h the cells were gently washed three times with PBS. The cells were trypsinated and collected. The resulting samples were centrifuged, and the supernatant removed. The pellets were digested with 200 μl of aqua regia overnight and then diluted in an analytical flask with water (final volume 10mL). Gold concentration was quantified by induced coupled plasma-mass spectroscopy (ICP-MS). Measurements were performed using an ICP-MS Perkin Elmer (NexION 300).

Author information

Corresponding Author

*E-mail: victor.puntes@icn2.cat

Acknowledgements

We acknowledge financial support from the Pandora European Training Network (GA-671881) funded in the framework of H2020 Marie Skłodowska-Curie ITN programme, Spanish Ministerio de Ciencia, Innovación y Universidades (MCIU) (RTI2018-099965-B-I00, AEI/FEDER,UE), and from the Catalan Agència de Gestió d'Ajuts Universitaris i de Recerca (AGAUR) (2017-SGR-1431). L.M. thanks the financial support from AGAUR by means of the Grants for the incorporation of post-doctoral research staff into the Catalan science and technology system within the Beatriu de Pinós program (Grant No. 2016 BP 00350). N.G.B. acknowledges financial support by MINECO through the Ramon y Cajal program (RYC-2012- 10991). ICN2 is supported by the Severo Ochoa program from Spanish MINECO (Grant No. SEV-2017-0706) and is funded by the CERCA Programme /Generalitat de Catalunya. The present work has been performed in the framework of the doctorate in Chemistry and Materials Science at the Autonomous University of Barcelona (UAB). O.H.M. acknowledges a financial support from the Spanish Ministry of Science and Innovation (MICINN) by a FPI fellowship, resolved by the Agencia Estatal de Investigación (AEI) with reference (BES-2017-083043).

References

1. Casals, E.; Pfaller, T.; Duschl, A.; Oostingh, G.J.; Puntes, V. Time evolution of the nanoparticle protein corona. *ACS Nano* **2010**, *4*, 3623–3632.
2. Ritz, S.; Schöttler, S.; Kotman, N.; Baier, G.; Musyanovych, A.; Kuharev, J.; Landfester, K.; Schild, H.; Jahn, O.; Tenzer, S. Protein corona of nanoparticles: distinct proteins regulate the cellular uptake. *Biomacromolecules* **2015**, *16*, 1311–1321.
3. Zhang, D.; Neumann, O.; Wang, H.; Yuwono, V.M.; Barhoumi, A.; Perham, M.; Hartgerink, J.D.; Wittung-Stafshede, P.; Halas, N.J. Gold nanoparticles can induce the formation of protein-based aggregates at physiological pH. *Nano Lett.* **2009**, *9*, 666–671.
4. Kelly, P.M.; Åberg, C.; Polo, E.; O'connell, A.; Cookman, J.; Fallon, J.; Krpetić, Ž.; Dawson, K.A. Mapping protein binding sites on the biomolecular corona of nanoparticles. *Nat. Nanotechnol.* **2015**, *10*, 472.
5. Casals, E.; Gonzalez, E.; Puntes, V.F. Reactivity of inorganic nanoparticles in biological environments: insights into nanotoxicity mechanisms. *J. Phys. D. Appl. Phys.* **2012**, *45*, 443001.

6. Dobrovolskaia, M.A.; McNeil, S.E. Immunological properties of engineered nanomaterials. *Nat. Nanotechnol.* **2007**, *2*, 469.
7. Tenzer, S.; Docter, D.; Kuharev, J.; Musyanovych, A.; Fetz, V.; Hecht, R.; Schlenk, F.; Fischer, D.; Kiouptsi, K.; Reinhardt, C. Rapid formation of plasma protein corona critically affects nanoparticle pathophysiology. *Nat. Nanotechnol.* **2013**, *8*, 772–781.
8. Saha, K.; Rahimi, M.; Yazdani, M.; Kim, S.T.; Moyano, D.F.; Hou, S.; Das, R.; Mout, R.; Rezaee, F.; Mahmoudi, M. Regulation of macrophage recognition through the interplay of nanoparticle surface functionality and protein corona. *ACS Nano* **2016**, *10*, 4421–4430.
9. Di Silvio, D.; Rigby, N.; Bajka, B.; Mackie, A.; Bombelli, F.B. Effect of protein corona magnetite nanoparticles derived from bread in vitro digestion on Caco-2 cells morphology and uptake. *Int. J. Biochem. Cell Biol.* **2016**, *75*, 212–222.
10. Monopoli, M.P.; Walczyk, D.; Campbell, A.; Elia, G.; Lynch, I.; Baldelli Bombelli, F.; Dawson, K.A. Physical− chemical aspects of protein corona: relevance to in vitro and in vivo biological impacts of nanoparticles. *J. Am. Chem. Soc.* **2011**, *133*, 2525–2534.
11. Lundqvist, M.; Stigler, J.; Elia, G.; Lynch, I.; Cedervall, T.; Dawson, K.A. Nanoparticle size and surface properties determine the protein corona with possible implications for biological impacts. *Proc. Natl. Acad. Sci.* **2008**, *105*, 14265–14270.
12. Barbero, F.; Russo, L.; Vitali, M.; Piella, J.; Salvo, I.; Borrajo, M.L.; Busquets-Fité, M.; Grandori, R.; Bastús, N.G.; Casals, E.; et al. Formation of the Protein Corona: The Interface between Nanoparticles and the Immune System. *Semin. Immunol.* 2017, *34*, 52–60.
13. Vroman, L. Effect of adsorbed proteins on the wettability of hydrophilic and hydrophobic solids. *Nature* **1962**, *196*, 476–477.
14. Vroman, L.; Adams, A.L. Identification of rapid changes at plasma–solid interfaces. *J. Biomed. Mater. Res.* **1969**, *3*, 43–67.
15. Vroman, L.; Adams, A.L. Findings with the recording ellipsometer suggesting rapid exchange of specific plasma proteins at liquid/solid interfaces. *Surf. Sci.* **1969**, *16*, 438–446.
16. Vroman, L.; Adams, A.L.; Klings, M. Interactions among human blood proteins at interfaces. In Proceedings of the Federation proceedings; 1971; Vol. 30, pp. 1494–1502.
17. Vroman, L.; Adams, A.L.; Fischer, G.C.; Munoz, P.C. Interaction of high molecular weight kininogen, factor XII, and fibrinogen in plasma at interfaces. **1980**.
18. Boraschi, D.; Alijagic, A.; Auguste, M.; Barbero, F.; Ferrari, E.; Hernadi, S.; Mayall, C.; Michelini, S.; Navarro Pacheco, N.I.; Prinelli, A.; et al. Addressing Nanomaterial Immunosafety by Evaluating Innate Immunity across Living Species. *Small* **2020**, 2000598, doi:10.1002/smll.202000598.

19. Swartzwelter, B.J.; Mayall, C.; Alijagic, A.; Barbero, F.; Ferrari, E.; Hernadi, S.; Michelini, S.; Navarro Pacheco, N.I.; Prinelli, A.; Swart, E. Cross-Species Comparisons of Nanoparticle Interactions with Innate Immune Systems: A Methodological Review. *Nanomaterials* **2021**, *11*, 1528.
20. Casals, E.; Pfaller, T.; Duschl, A.; Oostingh, G.J.; Puntes, V.F. Hardening of the nanoparticle–protein corona in metal (Au, Ag) and oxide (Fe3O4, CoO, and CeO2) nanoparticles. *Small* **2011**, *7*, 3479–3486.
21. Piella, J.; Bastús, N.G.; Puntes, V. Size-dependent protein–nanoparticle interactions in citrate-stabilized gold nanoparticles: the emergence of the protein corona. *Bioconjug. Chem.* **2017**, *28*, 88–97.
22. Madathiparambil Visalakshan, R.; González García, L.E.; Benzigar, M.R.; Ghazaryan, A.; Simon, J.; Mierczynska-Vasilev, A.; Michl, T.D.; Vinu, A.; Mailänder, V.; Morsbach, S. The influence of nanoparticle shape on protein corona formation. *Small* **2020**, *16*, 2000285.
23. Barbero, F.; Moriones, O.H.; Bastús, N.G.; Puntes, V. Dynamic Equilibrium in the Cetyltrimethylammonium Bromide–Au Nanoparticle Bilayer, and the Consequent Impact on the Formation of the Nanoparticle Protein Corona. *Bioconjug. Chem.* **2019**, *30*, 2917–2930, doi:10.1021/acs.bioconjchem.9b00624.
24. Fernández, A. Epistructural tension promotes protein associations. *Phys. Rev. Lett.* **2012**, *108*, 188102.
25. Maiorano, G.; Sabella, S.; Sorce, B.; Brunetti, V.; Malvindi, M.A.; Cingolani, R.; Pompa, P.P. Effects of cell culture media on the dynamic formation of protein− nanoparticle complexes and influence on the cellular response. *ACS Nano* **2010**, *4*, 7481–7491.
26. Sperling, R.A.; Gil, P.R.; Zhang, F.; Zanella, M.; Parak, W.J. Biological applications of gold nanoparticles. *Chem. Soc. Rev.* **2008**, *37*, 1896–1908.
27. Ghosh, P.; Han, G.; De, M.; Kim, C.K.; Rotello, V.M. Gold nanoparticles in delivery applications. *Adv. Drug Deliv. Rev.* **2008**, *60*, 1307–1315.
28. Roth, E.; Oehler, R.; Manhart, N.; Exner, R.; Wessner, B.; Strasser, E.; Spittler, A. Regulative potential of glutamine—relation to glutathione metabolism. *Nutrition* **2002**, *18*, 217–221.
29. INUI, K.; OREFFO, R.O.C.; T TRIFFITT, J. Effects of beta mercaptoethanol on the proliferation and differentiation of human osteoprogenitor cells. *Cell Biol. Int.* **1997**, *21*, 419–425.
30. Bastús, N.G.; Comenge, J.; Puntes, V. Kinetically controlled seeded growth synthesis of citrate-stabilized gold nanoparticles of up to 200 nm: size focusing versus Ostwald ripening. *Langmuir* **2011**, *27*, 11098–11105.

31. Al-Johani, H.; Abou-Hamad, E.; Jedidi, A.; Widdifield, C.M.; Viger-Gravel, J.; Sangaru, S.S.; Gajan, D.; Anjum, D.H.; Ould-Chikh, S.; Hedhili, M.N. The structure and binding mode of citrate in the stabilization of gold nanoparticles. *Nat. Chem.* **2017**, *9*, 890–895.
32. Liz-Marzán, L.M. Tailoring surface plasmons through the morphology and assembly of metal nanoparticles. *Langmuir* **2006**, *22*, 32–41.
33. Ghosh, S.K.; Pal, T. Interparticle coupling effect on the surface plasmon resonance of gold nanoparticles: from theory to applications. *Chem. Rev.* **2007**, *107*, 4797–4862.
34. Lévy, R.; Thanh, N.T.K.; Doty, R.C.; Hussain, I.; Nichols, R.J.; Schiffrin, D.J.; Brust, M.; Fernig, D.G. Rational and combinatorial design of peptide capping ligands for gold nanoparticles. *J. Am. Chem. Soc.* **2004**, *126*, 10076–10084.
35. Dos Santos, T.; Varela, J.; Lynch, I.; Salvati, A.; Dawson, K.A. Effects of transport inhibitors on the cellular uptake of carboxylated polystyrene nanoparticles in different cell lines. *PLoS One* **2011**, *6*, e24438.
36. Albanese, A.; Chan, W.C.W. Effect of gold nanoparticle aggregation on cell uptake and toxicity. *ACS Nano* **2011**, *5*, 5478–5489.
37. Cho, E.C.; Zhang, Q.; Xia, Y. The effect of sedimentation and diffusion on cellular uptake of gold nanoparticles. *Nat. Nanotechnol.* **2011**, *6*, 385–391.
38. Chithrani, B.D.; Ghazani, A.A.; Chan, W.C.W. Determining the size and shape dependence of gold nanoparticle uptake into mammalian cells. *Nano Lett.* **2006**, *6*, 662–668.
39. Vasir, J.K.; Labhasetwar, V. Quantification of the force of nanoparticle-cell membrane interactions and its influence on intracellular trafficking of nanoparticles. *Biomaterials* **2008**, *29*, 4244–4252.
40. Alkilany, A.M.; Murphy, C.J. Toxicity and cellular uptake of gold nanoparticles: what we have learned so far? *J. nanoparticle Res.* **2010**, *12*, 2313–2333.
41. Verdera, H.C.; Gitz-Francois, J.J.; Schiffelers, R.M.; Vader, P. Cellular uptake of extracellular vesicles is mediated by clathrin-independent endocytosis and macropinocytosis. *J. Control. Release* **2017**, *266*, 100–108.
42. Mayor, S.; Pagano, R.E. Pathways of clathrin-independent endocytosis. *Nat. Rev. Mol. cell Biol.* **2007**, *8*, 603–612.
43. Guilloteau, N.; Bienvenu, C.; Charrat, C.; Blanco, J.L.J.; Díaz-Moscoso, A.; Mellet, C.O.; Fernández, J.M.G.; Vierling, P.; Di Giorgio, C. Cell uptake mechanisms of glycosylated cationic pDNA–cyclodextrin nanoparticles. *RSC Adv.* **2015**, *5*, 29135–29144.
44. Alijagic, A.; Barbero, F.; Gaglio, D.; Napodano, E.; Benada, O.; Kofroňová, O.; Puntes, V.F.; Bastús, N.G.; Pinsino, A. Gold nanoparticles coated with polyvinylpyrrolidone and sea urchin

extracellular molecules induce transient immune activation. *J. Hazard. Mater.* **2021**, *402*, 123793.

45. Willets, K.A.; Van Duyne, R.P. Localized surface plasmon resonance spectroscopy and sensing. *Annu. Rev. Phys. Chem.* **2007**, *58*, 267–297.
46. Leff, D. V; Brandt, L.; Heath, J.R. Synthesis and characterization of hydrophobic, organically-soluble gold nanocrystals functionalized with primary amines. *Langmuir* **1996**, *12*, 4723–4730.

Supplementary Information

Interaction between AuNPs and CCM supplements.

To better understand the role and the properties of the CCM supplements, especially the PS, the mere relationship between AuNPs and the supplements was explored, studying their ability to interact with AuNPs. Four aqueous solutions of each single molecule were prepared at the typical standard concentration used in the cell cultures and AuNPs at concentration of $1.3 \cdot 10^{12}$ NPs/mL were diluted 1:10 into the solutions. Time evolution of the UV-vis spectra and Z potential of AuNPs were followed (Figure SI-1). UV-vis spectra of AuNPs exposed to an aqueous solution of GLN (2 mM, phosphate buffer 10 mM, pH 7.4) showed immediately after the exposition a 2 nm red-shifts of the LSPR which can be ascribed to the change of the refractive index at the vicinity of the NPs surface (Figure SI-1B). Coupled with a decrease in the Z potential (Figure SI-1E), the results pointed out the ability of GLN to interact with the NPs. The potential interacting group were the amine and carboxyl functional groups, chemical moieties that are reported to have the ability to form weak interaction with gold surface [31,46]. The change in Z potential was consistent with a GLN overall slightly negative charge at the working pH, presenting an isoelectric point of 5.7.

The UV-vis spectra of AuNPs mixed with an aqueous solution of BME (50 μM, phosphate buffer 10 mM, pH 7.4) showed already at time 0 the appearance of a second peak at around 800 nm associated to the inter-particle plasmon coupling during AuNPs aggregation [33] (Figure SI-1C). The essentially unchanged LSPR band profile overtime suggested the formation of NP aggregates that once formed basically did not continue to evolve overtime, maintaining a colloidal nature. As expected BME, presenting a thiol group was able to interact with NPs gold surface partially replacing the citrate and presenting a really short alkyl chain and no charged moieties the resulting surface was not able to give

enough repulsive force to fully stabilize the system. Decrease in the Z potential was in line with a partial replacement of the citrate for neutral moieties.

Figure SI-1A shows the results for the exposition of AuNPs to a solution of PhR (44.8 μM, phosphate buffer 10 mM, pH 7.4), due to the strong light absorption of the pH sensitive dye in the same range of the NPs, the spectra were recorded after a centrifugal purification of the sample. The LSPR band profile of the particles did not shows significant differences after the exposition and the Z potential value presented a small decrease; to further characterize the system, NPs colloidal stability against saline media were tested. AuNPs before and after the exposition to PhR were exposed to a growing concentration of NaCl, from 10 to 100 mM, and the UV-vis spectra were recorded at time 0. The extent of aggregation was systematically quantified from UV-vis spectra, by calculating the aggregation parameter (AP) according to Lévy et al. [34], basically related to the extent of the second plasmonic peak. AP values higher than 0.5 indicated significant aggregation. The results showed that once exposed to PhR, AuNPs present higher stability against ionic strength that could be correlated with an interaction of the dye with the surface of the particle that conferred a partial stabilizing steric repulsion component in addition to the electrostatic one. The three aromatic rings, the sulphate group and the ketone composing the PhR could be responsible for the interaction with the gold surface. It could be further hypothesised that the polyaromatic structure was responsible for the observed partial steric repulsion properties.

Figure SI1-D shows the UV-vis profile over time of AuNP exposed to PS (100 U/mL (~170 μM) penicillin, 172 μM streptomycin). A classic AuNPs aggregation LSPR band profile was observed a time 0, after 24 h almost no absorption spectrum was observed, ascribable to the formation of macro aggregates of NPs that had sedimented. The Z potential of the NPs/PS solution presents a slightly positive value. The NPs aggregation and an almost neutral Z potential suggested an aggregation led by the cationic streptomycin.

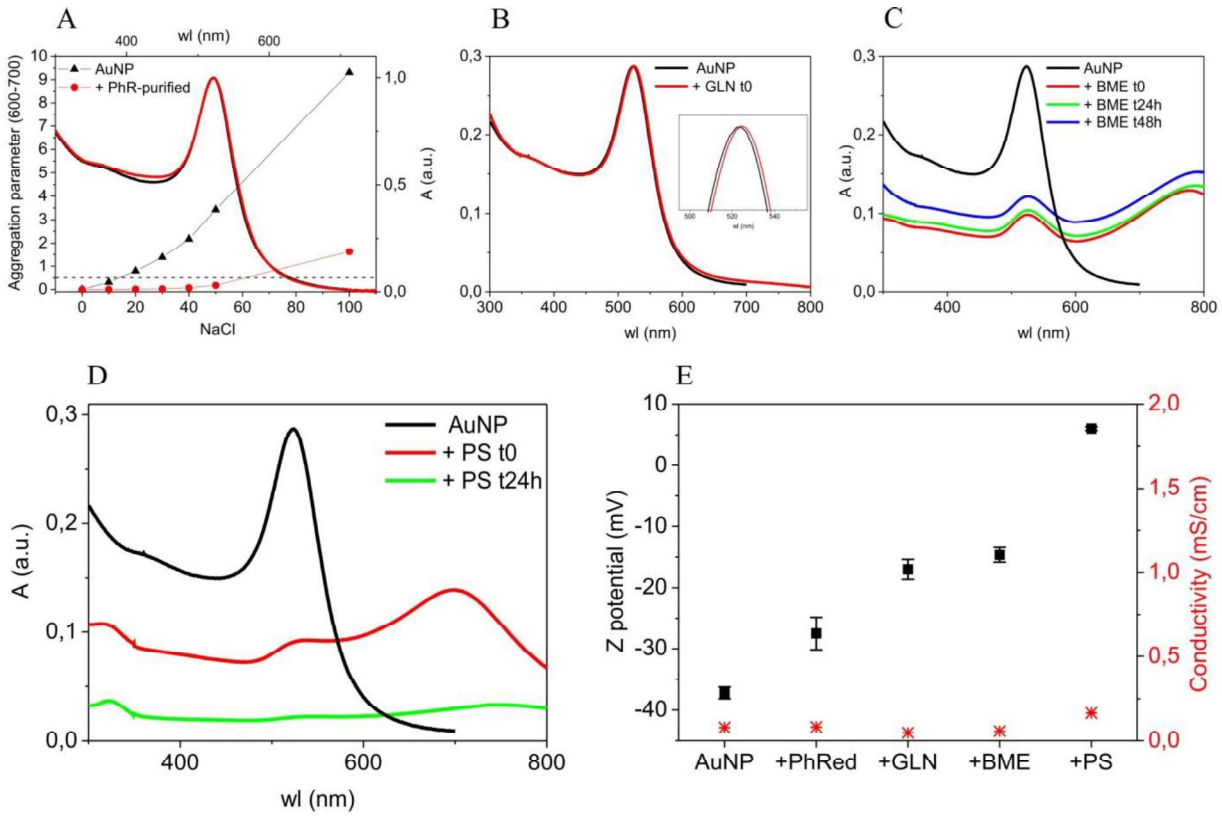

Figure SI 1. 25nm AuNPs diluted 1:10 in aqueouse solutions of: Phenol Red (PhR); L-glutamine (GLN); β-mercaptoethanol (BME); Penicillin/Streptomycin (PS). (**A**): UV-vis spectra of AuNPs (black), UV-vis spectra of Au NPs exposed to a PhR solution and subsequently purified (red); Experimentally measured Aggregation Parameters (AP) of AuNPs versus growing concentration of NaCl (black triangle) and AP of AuNPs exposed to PhR and subsequently purified versus a growing concentration of NaCl (red circles). (**B**): UV-vis spectra of Au NPs (black), UV-vis spectra of AuNPs after the exposition to GLN solution (red). (**C**): UV-vis spectra of Au NPs (black), UV-vis spectra of Au NPs exposed to a BME solution, time 0 (red), time 24h (green), time 48h (blue). (**D**): UV-vis spectra of Au NPs (black), UV-vis spectra of Au NPs exposed to a Penicillin/Streptomycin solution, time 0 (red), time 24h (green). (**E**): Z potential (black square) and Conductivity (red stars) of all the previous samples at time 0 of exposition.

Protein-stabilized AuNPs aggregates.

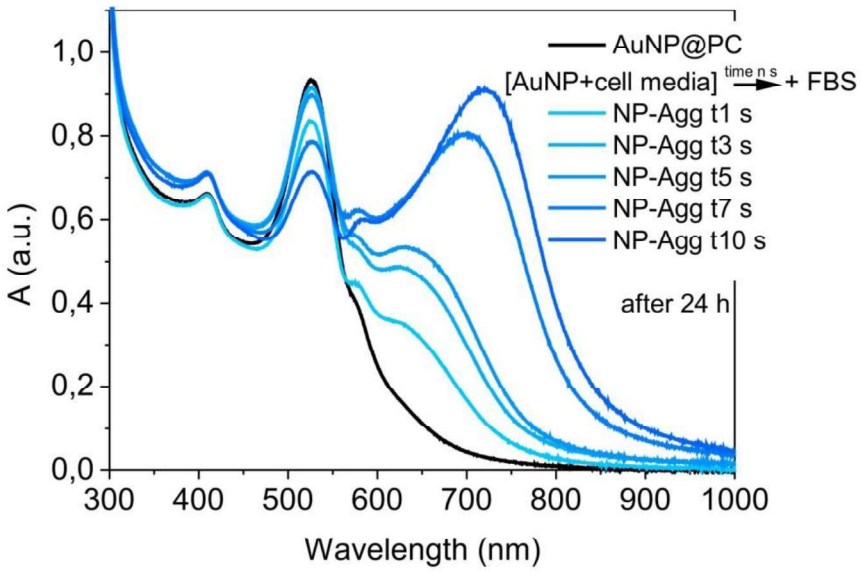

Figure SI 2. UV-vis spectroscopy of protein-stabilized AuNPs aggregates. Five samples of AuNPs ($2.7 \cdot 10^{12}$ NPs/mL) were diluted 1:10 into cell culture media, after 1, 3,5,7 and 10 s FBS (10%) was added to the mixture. The figure shows the spectra of each sample after 24 h. The base line was performed with a solution of cell culture media containing phenol red. The small shoulder approximately at 600 nm was due to a not perfect subtraction of the signal of the phenol red.